

Subscriber access provided by RENSSELAER POLYTECH INST

Energy, Environmental, and Catalysis Applications

Rational Designed Mixed-Conductive Sulfur Cathodes for All-Solid-State Lithium Batteries

Jie Yue, Yonglin Huang, Sufu Liu, Ji Chen, Fudong Han, and Chunsheng Wang

ACS Appl. Mater. Interfaces, Just Accepted Manuscript • DOI: 10.1021/acsami.0c08564 • Publication Date (Web): 20 Jul 2020

Downloaded from pubs.acs.org on July 25, 2020

Just Accepted

"Just Accepted" manuscripts have been peer-reviewed and accepted for publication. They are posted online prior to technical editing, formatting for publication and author proofing. The American Chemical Society provides "Just Accepted" as a service to the research community to expedite the dissemination of scientific material as soon as possible after acceptance. "Just Accepted" manuscripts appear in full in PDF format accompanied by an HTML abstract. "Just Accepted" manuscripts have been fully peer reviewed, but should not be considered the official version of record. They are citable by the Digital Object Identifier (DOI®). "Just Accepted" is an optional service offered to authors. Therefore, the "Just Accepted" Web site may not include all articles that will be published in the journal. After a manuscript is technically edited and formatted, it will be removed from the "Just Accepted" Web site and published as an ASAP article. Note that technical editing may introduce minor changes to the manuscript text and/or graphics which could affect content, and all legal disclaimers and ethical guidelines that apply to the journal pertain. ACS cannot be held responsible for errors or consequences arising from the use of information contained in these "Just Accepted" manuscripts.

Rational Designed Mixed-Conductive Sulfur

Cathodes for All-Solid-State Lithium Batteries

Jie Yue[†], Yonglin Huang[‡], Sufu Liu[†], Ji Chen[†], Fudong Han*[‡], Chunsheng Wang*[†]

†Department of Chemical and Biomolecular Engineering, University of Maryland, College Park, Maryland, 20742, United States

[‡]Department of Mechanical, Aerospace, and Nuclear Engineering, Rensselaer Polytechnic Institute, Troy, New York, 12180, United States

Keywords: sulfur cathode, mixed conductive, solid electrolyte, battery, composite

ABSTRACT All-solid-state lithium-sulfur batteries (ASSLSBs) hold great promise for safe and high-energy-density energy storage. However, developing high-performance sulfur cathodes has been proven difficult due to low electronic and ionic conductivities and large volume change of sulfur during charge and discharge. Here, we reported an approach to synthesize sulfur cathodes with a mixed electronic and ionic conductivity by infiltrating a solution consisting of Li₃PS₄ (LPS) solid electrolyte and S active material into a mesoporous carbon (CMK-3). This approach leads to a uniform dispersion of amorphous Li₃PS₇ (L3PS) catholyte in an electronically conductive carbon matrix, enabling high and balanced electronic/ionic conductivities in the cathode composite. The inherent porous structure of CMK-3 also helps to accommodate the strain/stress generated during

the expansion and shrinkage of the active material. In sulfide-based all-solid-state batteries with Li metal as the anode, this cathode composite delivered a high capacity of 1025 mAh g⁻¹ after 50 cycles at 60 °C at 1/8 °C. This work highlights the important role of high and balanced electronic and ionic conductivities in developing high-performance sulfur cathodes for ASSLSBs.

INTRODUCTION

The ever-increasing demand on the energy density has posed a serious concern on the safety of today's lithium ion batteries. All-solid-state batteries using nonflammable solid electrolytes are being considered as a promising solution for safer batteries. It is known that the maximum energy density of a solid-state battery is determined by the cathode composite for a fixed capacity ratio of negative to positive electrodes (N/P ratio) and a fixed amount of solid electrolyte. Sulfur, because of its high thermotical capacity, has received intense research interest as the cathode active material. A recent analysis by Janek also pointed out that with a 50-µm thick solid electrolyte, sulfur is the only cathode that can enable a solid-state battery with exceptionally high energy density beyond 500 Wh kg⁻¹. Nevertheless, developing sulfur cathodes with a high performance in terms of sulfur utilization, cycle life and rate performance is very challenging due to (i) the insulating nature of sulfur for both electrons and ions and (ii) the large volume change of sulfur (80%) during lithiation/delithiation. In

Inspired by the success of liquid-electrolyte Li-S batteries, ¹² tremendous efforts have been done to improve the electronic conductivity of sulfur cathodes by introducing various electronically conductive additives such as copper, ^{13,14} acetylene black, ¹⁵ carbon nanofibers, ¹⁶ reduced graphene oxide, ¹⁷ and graphite ¹⁸. However, the performance improvement in ASSLSBs is not as effective as that in the liquid-electrolyte Li-S batteries. Such a difference is mainly caused by the different

property of solid electrolytes and liquid electrolytes. Unlike liquid electrolytes that are infiltrative and flowable, solid electrolytes are usually fixed at their positions once the cathode has been prepared. As a result, the ionic conduction percolation in the cathode composite is much harder to achieve in solid-state batteries than that in the liquid electrolyte batteries. In order to improve the ionic conductivity of the electrodes, several lithium superionic sulfides such as lithium polysulfidophosphate¹⁹ and Li₃PS₄ (LPS) coated Li₂S²⁰ were fabricated by Liang et al as the cathodes for ASSLSBs. These superionic sulfides were then mixed with carbon and binder to make the mixed conductive cathode composites. Despite apparent improvement in the cycling stability (>100 cycles), these superionic cathodes are usually tested with a low loading of active material (0.25-0.60 mg cm⁻²). ^{19,20} One main reason for the limited performance improvement is that most of the above-mentioned work only focused on improving one conductivity at nano-scale, either electronic or ionic, in the cathode composite, while for an ideal cathode both electronic and ionic conductivities should be ensured at nano-scale for a high utilization of sulfur. In addition to this, the huge stress/strain caused by the volume change of sulfur during operation has not been addressed, which will certainly affect the performance improvement. 11,21,22

In this work, we developed a nano-scale mix-conducive sulfur cathode for all-solid-state lithium batteries. By infiltrating a solution with highly ionic conductive Li₃PS₇ (L3PS) active material into mesoporous carbon CMK-3, we were able to fabricate a cathode with both high and balanced ionic and electronic conductivities and with an inherent porous structure to accommodate the volume change of active materials. The cathode composite exhibit excellent cycling and rate performance in an all-solid-state lithium battery even with no additional solid electrolyte and carbon added in the electrode.

EXPERIMENTAL SECTION

Material Synthesis: Li₃PS₄ glass solid electrolyte was prepared by a mechanical milling process. In brief, 75 mol % of lithium sulfide (Li₂S, Sigma-Aldrich) and 25 mol % of phosphorus pentasulfide (P₂S₅, Sigma-Aldrich) were mixed in a zirconia pot at a fixed rotation speed of 510 rpm for 45 h.³⁰ To prepare L3PS-CMK-3 composite, a mixture of 0.18 g Li₃PS₄ glass solid electrolyte and 0.096 g sulfur (S, Sigma-Aldrich) was dissolved in 6 mL Tetrahydrofura (THF, Sigma-Aldrich) solvent, while 0.096 g ordered mesoporous carbon (CMK-3, ACS Material) powders were dispersed in another 6 mL THF solvent. After that, these two solutions were mixed together and stirred overnight. All the above processes were conducted under Argon. The mixed solution was then dried at 80 °C for 24 h under vacuum to completely remove THF solvent, and the L3PS-CMK-3 composite was obtained. A composite of S, Li₃PS₄ glass solid electrolyte and CMK-3 (demoted as 3S-LPS-CMK-3) with the same weight ratio was also prepared by a ball-milling method (370 rpm for 1h) as a control sample.

Material Characterization: XRD patterns were obtained using a D8 Advance X-ray diffractometer (Bruker AXS, WI, USA) with Cu Kα radiation. A 532 nm diode-pumped solid-state laser was used on a Horiba Jobin Yvon Labram Aramis to record Raman spectra. To characterize the morphologies of samples, TEM images and SEM images were examined with transmission electron microscopy (TEM, JEM 2100 LaB6) and scanning electron microscopy (SEM, Hitachi SU-70), separately. N₂ adsorption/desorption isotherms were measured with Micromeritics ASAP 2020 Porosimeter Test Station. Surface areas were calculated with the Brunauer-Emmett-Teller (BET) method, and pore volume distribution was obtained using the Barrett-Joyner-Halenda (BJH) equation.

Electrochemical Measurement: All solid-state lithium-sulfur batteries were fabricated using Li₃PS₄ glass as the solid electrolyte, Li metal as the anode, and L3PS–CMK-3 or 3S–LPS–CMK-3 as the cathode composite. The ionic conductivities of L3PS at different temperatures were measured using an ion-blocking Pt/L3PS/Pt cell. The cell was fabricated by pressing 150 mg L3PS powders into pellets, followed by sputtering of Pt. Then, electrochemical impedance spectra (EIS) were measured at different temperatures. To assemble all solid-state lithium-sulfur batteries, 150 mg Li₃PS₄ glass were put in a PTFE tank with a diameter of 1 cm, and 5 mg L3PS–CMK-3 composite or 3S–LPS–CMK-3 composite was presses on top of the solid electrolyte under 360 MPa. Then, lithium metal was attached directly on the other side of the solid electrolyte layer. All electrochemical performances including cycling properties and rate performances were tested using LAND CT-2001A battery cyclers within 1.2-3.0 V at 60 °C. EIS spectra of all solid-state lithium-sulfur batteries were measured using Solartron workstation in a frequency range 1 MHz-0.1 Hz with 20 mV AC amplitude.

RESULTS AND DISCUSSION

Figure 1a demonstrates the synthesis process for L3PS–CMK-3 composite. First, CMK-3 powders were dispersed in THF solvent, and LPS glass and S with a molar ratio of 1:3 were dissolved in another THF solvent. These two solutions were then mixed together and dried under vacuum to get L3PS–CMK-3 composite. Figure 1b shows the XRD patterns of S, LPS glass and L3PS–CMK-3 composite. The XRD pattern of L3PS–CMK-3 in Figure 1b indicates the amorphous structure of composite and no peaks for S can be observed, while the broad peak at around 18 degree that is

observed in the XRD patterns of both LPS and L3PS-CMK-3 is due to the sample holder for the measurement. The result shows LPS has completed reacted with active S forming a single amorphous phase, consistent with the study by Liang et al.¹⁹

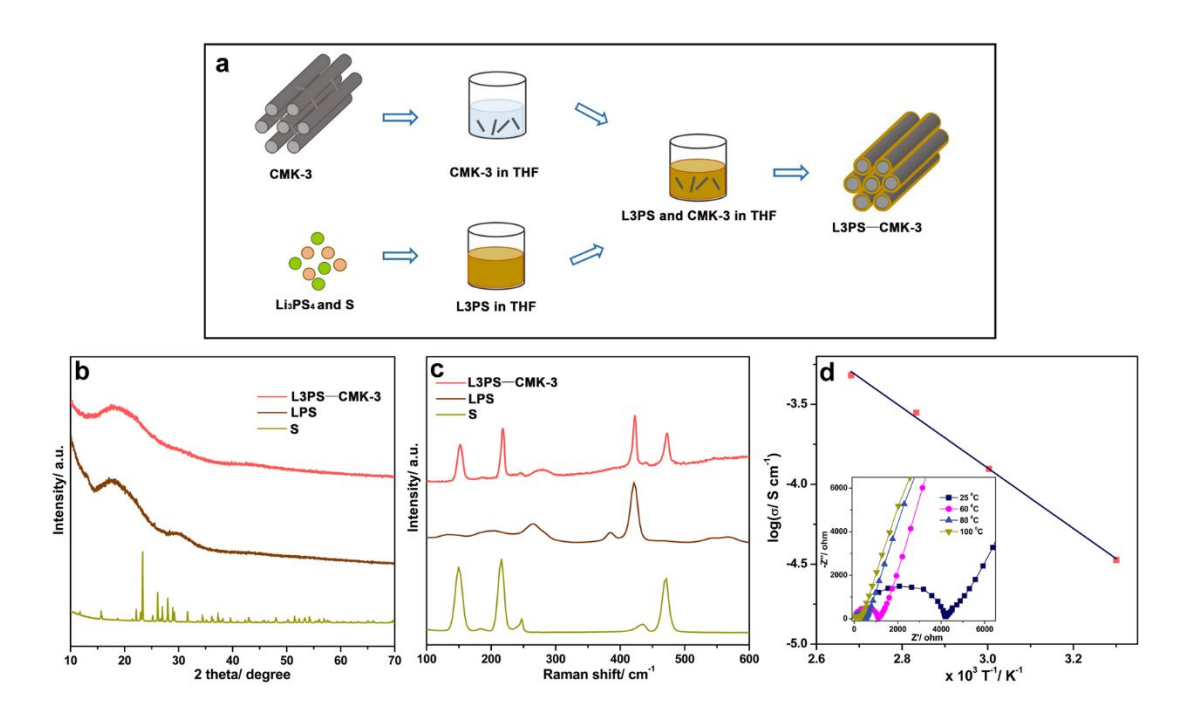


Figure 1. (a) Schematic synthesis process for the fabrication of L3PS-CMK-3 composite. (b) XRD patterns and (c) Raman spectra of S, LPS and L3PS-CMK-3. (d) Arrhenius plots and electrochemical impedance spectra at different temperatures (inset) of L3PS.

The Raman spectra of the L3PS-CMK-3 composite consist of chemical signatures of both LPS and S, implying that L3PS can be used as both an solid electrolyte and a cathode active material, i.e. a catholyte. The ionic conductivity of L3PS was also measured from electrochemical impedance spectra of a Pt/L3PS/Pt cell at different temperatures. The Arrhenius plot and the

impedance plot at different temperatures are shown in Figure 1d. The activation energy for L3PS is calculated to be 0.376 eV, and its ionic conductivity can reach 1.25×10⁻⁴ S cm⁻¹ at 60 °C, which is close to previous report.¹⁹

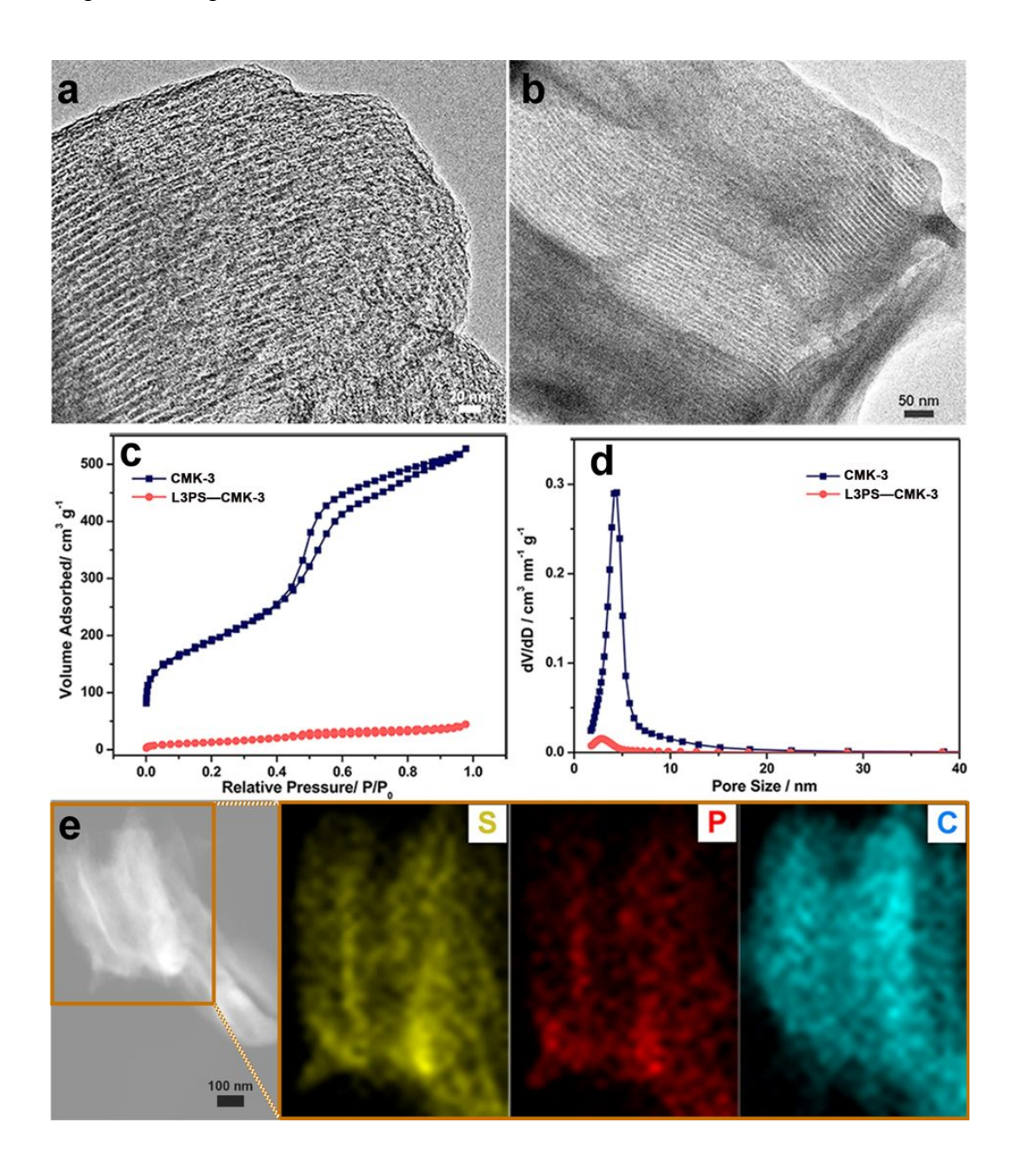


Figure 2. HRTEM images of (a) CMK-3 and (b) L3PS-CMK-3 composite. (c) N₂ adsorption/desorption isotherms and (d) BJH pore size distributions for CMK-3 and L3PS-CMK-3. (e) TEM image and corresponding elemental mappings of S, P and C in L3PS-CMK-3 composite.

Figures 2a and 2b compare the HRTEM images of CMK-3 and L3PS-CMK-3 composite, respectively. While a clear channel structure can be observed in the HRTEM image of CMK-3, the channels seem to be filled after infiltrating with L3PS. The infiltration of L3PS inside the pores of CMK-3 is also supported by the reduced surface area (Figure 2c), and more importantly, by the reduced pore size (Figure 2d) of L3PS-CMK-3 when comparing with pure CMK-3. Figure 2e displays the elemental mappings in L3PS-CMK-3 composite. A homogenous distribution of S, P and C can be easily observed in the composite, further confirming that L3PS was uniformly filled in the CMK-3 carbon matrix. The uniform distribution of L3PS in CMK-3 is also supported by the SEM images (Figure S1). A much more homogeneous distribution of S, P and C can be observed in L3PS-CMK-3 than in the 3S-LPS-CMK-3 cathode composite prepared by ball-milling S, LPS and CMK-3 with the same weight ratio as the SEM image and elemental mappings (Figure S2), TEM image (Figure S3) and XRD pattern (Figure S4) of 3S-LPS-CMK-3 indicate that it is mainly a composite of the three phases.

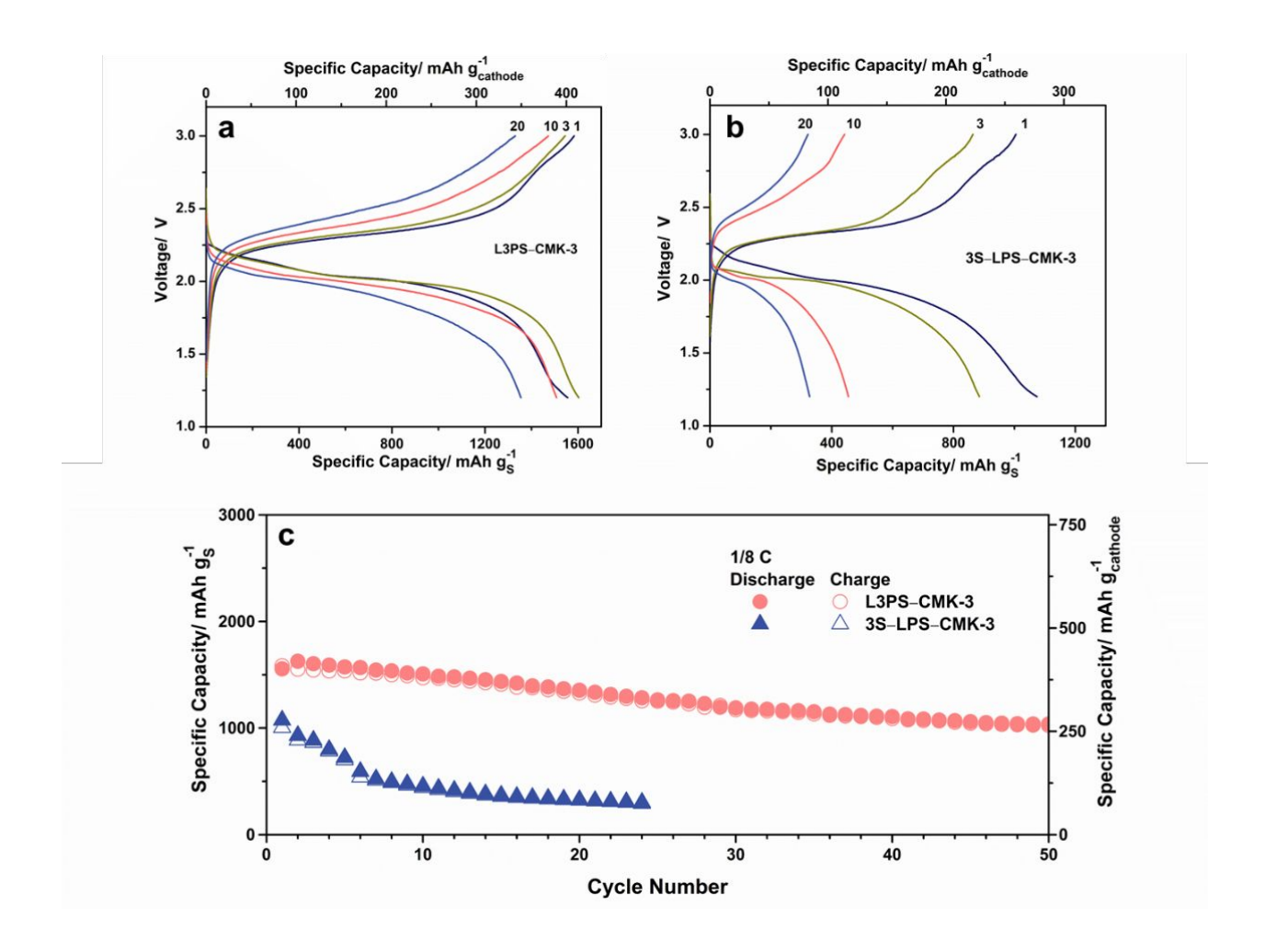


Figure 3. Electrochemical performances of L3PS–CMK-3 and 3S–LPS–CMK-3 composites in all solid-state lithium-sulfur batteries at 60 °C between 1.2 V and 3.0 V. The specific capacities were calculated based on the weight of sulfur and the total weight of the cathode composite. Charge-discharge curves at different cycles for (a) L3PS–CMK-3 and (b) 3S–LPS–CMK-3 composite cathodes at a current density of 1/8 C (1C = 1675 mA g⁻¹). (c) Cycling performances of L3PS–CMK-3 and 3S–LPS–CMK-3 composite cathodes at a current density of 1/8 C.

The electrochemical performances of L3PS-CMK-3 and 3S-LPS-CMK-3 composite cathodes were tested in all solid-state lithium-sulfur batteries using LPS glass as the solid electrolyte and Li as the anode between 1.2 V and 3 V at 60 °C. Figure 3a shows the charge-discharge profiles of L3PS-CMK-3 cathode at a current density of 1/8 C (1C=1675 mA g⁻¹). Only one plateau (2.0 V for the discharge process and 2.2 V for the charge process) can be observed, which is consistent with the binary (between Li₂S and S) phase transition during cycling, ^{19,23} although the reversible decomposition of solid electrolyte should also occur and contribute slightly to the capacity of the cathode composite.^{24,25} Compared with the charge-discharge curves of 3S-LPS-CMK-3 composite in Figure 3b, a higher specific capacity can be observed for the L3PS-CMK-3 cathode. Also, L3PS-CMK-3 exhibits smaller overpotentials than 3S-LPS-CMK-3 composite cathode, especially after more than three cycles, indicating better kinetics in L3PS-CMK-3 composite. Correspondingly, much better cycling stability for L3PS-CMK-3 composite can be obviously observed in Figure 3c. At the current density of 1/8 C, 3S-LPS-CMK-3 composite presents a reversible specific capacity of 1004 mAh g⁻¹ in the first cycle, and the capacity quickly decays to 322 mAh g⁻¹ within twenty cycles. However, the L3PS-CMK-3 composite delivers a much high reversible specific capacity of 1583 mAh g⁻¹ in the first cycle and the specific capacity maintains 1025 mAh g⁻¹ after 50 cycles. No apparent segregation of active material can be observed in the cathode composite (Figure S6), indicating the excellent stability of L3PS-CMK-3 during charge

and discharge processes. In addition, we also tested the performance of the cathode with higher S content. Figure S7 shows the charge/discharge curves and cycling performances of the L3PS–CMK-3, L3.67PS–CMK-3 and L4.33PS–CMK-3, where L3PS, L3.67PS and L4.33PS correspond to the molar ratio of 1:3, 1:4 and 1:5 between Li₃PS₄ and S. L3PS–CMK-3 shows much higher capacities than L3.67PS–CMK-3 and L4.33PS–CMK-3 over 50 cycles probably due to a well-balanced electronic conductivity and ionic conductivity and therefore is selected in this work. It should be noted that the S content in the L3PS–CMK-3 cathode is comparable with or even higher than the previous reports^{15,26-29}, highlighting the important role of high and balanced electronic and ionic conductivities in developing the S cathode composite.

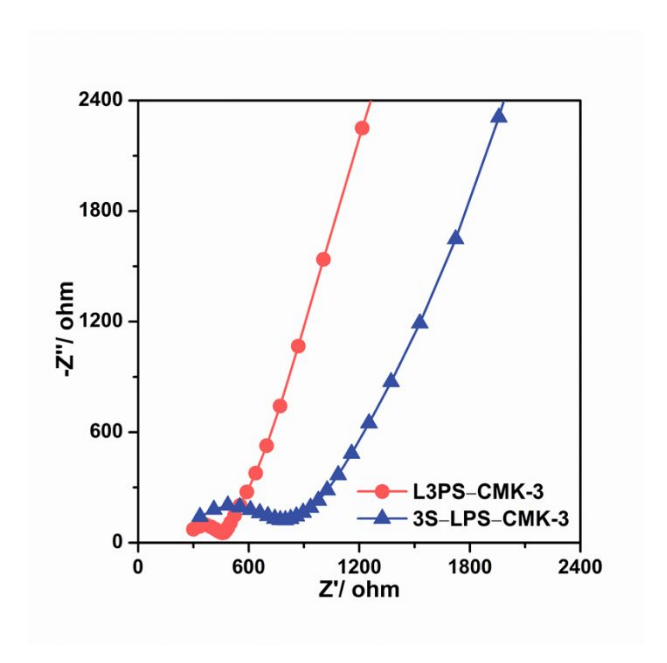


Figure 4. Electrochemical impedance spectra for the all-solid-state Li cells using L3PS–CMK-3 composite and 3S–LPS–CMK-3 composite as the cathodes. Both cells were fully discharged and charged for three cycles prior to the EIS test.

Figure 4 shows the impedance plots of all-solid-state batteries using L3PS-CMK-3 composite and 3S-LPS-CMK-3 composite as the cathode. Each EIS curve is consisted of one semicircle in the high-frequency region and one slope in the low-frequency region. The semicircle corresponds to the interfacial resistance from the anode/electrolyte interface and the cathode/electrolyte interface. Since all anodes are same anode, the difference in the interfacial resistance of these two cells could be mainly attributed to the interfacial resistance between the cathode and solid electrolyte. The result demonstrates a much better kinetics of the L3PS-CMK-3 composite than that of the 3S-LPS-CMK-3 composite. Since we are using exactly the same active material, solid electrolyte, and electronic conductive additive with exactly the same weight ratio in the two cathodes, the enhanced kinetics is mainly caused by higher conductivities (both electronic and ionic) due to a more uniform distribution of active material, ionic conductive material and electronic conductive material at the nanoscale in the L3PS-CMK-3 composite, as is supported by the higher conductivity of a single-phase L3PS than that of a 3S-LPS composite.

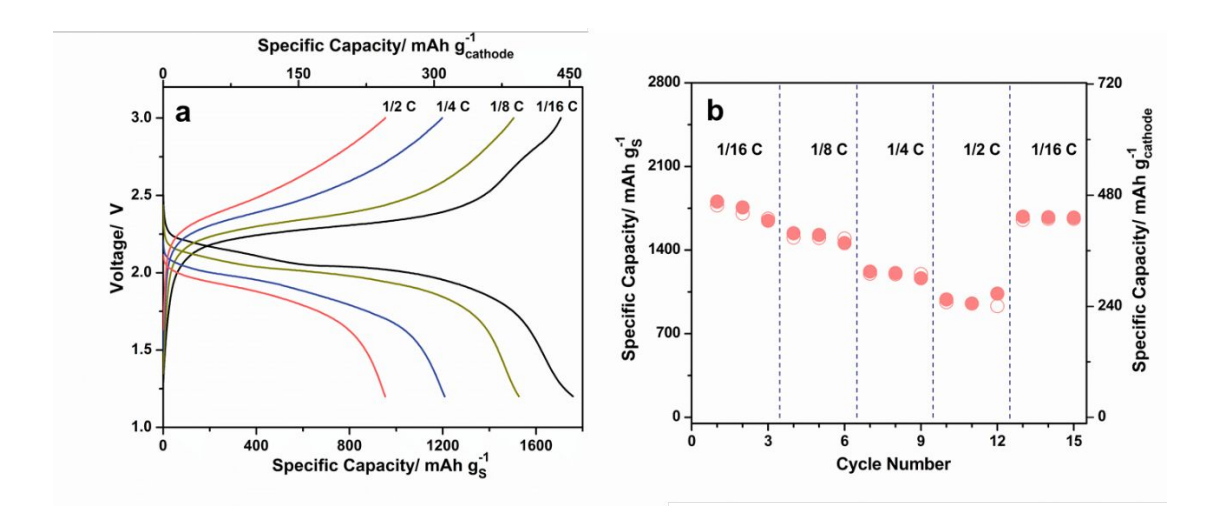


Figure 5. (a) Charge-discharge curves of the L3PS-CMK-3 cathode composite at different current densities and (b) corresponding rate performance of the L3PS-CMK-3 cathode composite. The specific capacities were calculated based on the weight of sulfur and the total weight of the cathode composite. These cells were discharged and charged at various current densities from 1/16 C to 1/2 C at 60 °C between 1.2 V and 3.0 V.

We then tested the rate performance of the L3PS–CMK-3 composite cathode between 1.2 V and 3 V at 60 °C. The cell was cycled at various current densities from 1/16 C to 1/2 C. At each current density, the cell was discharged and charged for three cycles. Charge-discharge curves at different current densities were given in Figure 5a, and the rate capacity was shown in Figure 5b. The L3PS–CMK-3 cathode could deliver reversible capacities of 1759 mAh g⁻¹, 1527 mAh g⁻¹, 1208 mAh g⁻¹ and 953 mAh g⁻¹ at current densities of 1/16 C (0.18 mA cm⁻²), 1/8 C (0.35 mA cm⁻²), 1/4 C (0.69 mA cm⁻²) and 1/2 C (1.38 mA cm⁻²), respectively. Therefore, L3PS–CMK-3 composite also

presents excellent rate performance even though no additional solid electrolyte and carbon were added in the electrode. The high utilization of S and excellent rate performance can be ascribed to the uniform distribution of active material, solid electrolyte and carbon which leads to high and balanced ionic and electronic conductivities in the cathode composites. Additionally, the inherent porous structure of CMK-3 can also buffer the volume change generated during charge-discharge processes, which helps improve the cycling stability.

CONCLUSIONS

In summary, a mixed-conductive composite of L3PS–CMK-3 was prepared by infiltrating L3PS (chemical composition: Li₃PS₇) catholyte into mesoporous CMK-3. This approach results in intimate contacts between active material, solid electrolyte and carbon and thus leads to a high and balanced mixed conductivity in the cathode composite. In addition, the porous carbon matrix can accommodate the strain/stress during cycling. The cathode composite exhibited to excellent cycling stability (1025 mAh g⁻¹ after 50 cycles) and rate performance up to 1/2 C in all solid-state lithium-sulfur battery at 60 °C. While the rate performance of the cathode has been improved largely due to the enhanced ionic and electronic conductivities, the cycling performance of the mixed conductive cathode is still limited. Further work is needed to understand more about the degradation mechanism of this cathode composite.

ASSOCIATE CONTENT

Supporting Information. Electronic supplementary information (ESI) available: SEM images and corresponding elemental mappings for L3PS–CMK-3 composite; SEM image and elemental

mappings, TEM image, and XRD pattern of 3S–LPS–CMK-3 composite; XRD patterns of 3S–LPS and L3PS; SEM image and elemental mappings of 3S–LPS–CMK-3 after charging and discharging; electrochemical performance of cathode composites with different molar ratio between Li3PS4 and S during synthesis; ionic conductivities of 3S–LPS and L3PS.

AUTHOR INFORMATION

Corresponding Authors

*Email: hanf2@rpi.edu

*Email: cswang@umd.edu

ACKNOWLEDGMENT

C.W. and F.H. gratefully acknowledge support by the National Science Foundation (Award No. 1805159) and the U.S. Department of Energy ARPA-E (Award No. DE-AR0000781).

REFERENCES

- (1) Janek, J.; Zeier, W. G.: A Solid Future for Battery Development. *Nat. Energy* **2016**, *1*, 16141.
- (2) Robinson, A. L.; Whittingham, M. S.: Pushing the Frontiers of Lithium-Ion Batteries Raises Safety Questions. *MRS Bull.* **2016**, *41*, 188-189.

- (3) Schnell, J.; Gunther, T.; Knoche, T.; Vieider, C.; Kohler, L.; Just, A.; Keller, M.; Passerini, S.; Reinhart, G.: All-Solid-State Lithium-Ion and Lithium Metal Batteries Paving the Way to Large-Scale Production. *J. Power Sources* **2018**, *382*, 160-175.
- (4) Mauger, A.; Armand, M.; Julien, C. M.; Zaghib, K.: Challenges and Issues Facing Lithium Metal for Solid-State Rechargeable Batteries. *J. Power Sources* **2017**, *353*, 333-342.
- (5) Hayashi, A.; Sakuda, A.; Tatsumisago, M.: Development of Sulfide Solid Electrolytes and Interface Formation Processes for Bulk-Type All-Solid-State Li and Na Batteries. *Front. Energy Res.* **2016**, *4*, 25.
- (6) Luntz, A. C.; Voss, J.; Reuter, K.: Interfacial Challenges in Solid-State Li Ion Batteries. *J. Phys. Chem. Lett.*, **2015**, *6*, 4599-4604.
- (7) McCloskey, B. D.: Attainable Gravimetric and Volumetric Energy Density of Li–S and Li Ion Battery Cells with Solid Separator-Protected Li Metal Anodes. *J. Phys. Chem. Lett.*, **2015**, *6*, 4581-4588.
- (8) Betz, J.; Bieker, G.; Meister, P.; Placke, T.; Winter, M.; Schmuch, R.: Theoretical Versus Practical Energy: A Plea for More Transparency in the Energy Calculation of Different Rechargeable Battery Systems. *Adv. Energy Mater.*, **2019**, *9*, 1803170.
- (9) Yan, M.; Wang, W.-P.; Yin, Y.-X.; Wan, L.-J.; Guo, Y.-G.: Interfacial Design for Lithium-Sulfur Batteries: from Liquid to Solid. *EnergyChem* **2019**, *I*, 100002.
- (10) Randau, S.; Weber, D. A.; Kotz, O.; Koerver, R.; Braun, P.; Weber, A.; Ivers-Tiffee, E.; Adermann, T.; Kulisch, J.; Zeier, W. G.; Richter, F. H.; Janek, J.: Benchmarking the Performance of All-Solid-State Lithium Batteries. *Nat. Energy*, **2020**, *5*, 259-270.
- (11) Barai, P.; Mistry, A.; Mukherjee, P. P.: Poromechanical Effect in the Lithium–Sulfur Battery Cathode. *Extreme Mech. Lett.*, **2016**, *9*, 359-370.

- (12) Ji, X. L.; Lee, K. T.; Nazar, L. F.: A Highly Ordered Nanostructured Carbon-Sulphur Cathode for Lithium-Sulphur Batteries. *Nat. Mater.*, **2009**, *8*, 500-506.
- (13) Hayashi, A.; Ohtsubo, R.; Tatsumisago, M.: Electrochemical Performance of All-Solid-State Lithium Batteries with Mechanochemically Activated Li₂S–Cu Composite Electrodes. *Solid State Ion.* **2008**, *179*, 1702-1705.
- (14) Hayashi, A.; Ohtomo, T.; Mizuno, F.; Tadanaga, K.; Tatsumisago, M.: All-Solid-State Li/S Batteries with Highly Conductive Glass–Ceramic Electrolytes. *Electrochem. Commun.* **2003**, *5*, 701-705.
- (15) Kobayashi, T.; Imade, Y.; Shishihara, D.; Homma, K.; Nagao, M.; Watanabe, R.; Yokoi, T.; Yamada, A.; Kanno, R.; Tatsumi, T.: All Solid-State Battery with Sulfur Electrode and thio-LISICON Electrolyte. *J. Power Sources* **2008**, *182*, 621-625.
- (16) Yamada, T.; Ito, S.; Omoda, R.; Watanabe, T.; Aihara, Y.; Agostini, M.; Ulissi, U.; Hassoun, J.; Scrosati, B.: All Solid-State Lithium–Sulfur Battery Using a Glass-Type P₂S₅–Li₂S Electrolyte: Benefits on Anode Kinetics. *J. Electrochem. Soc.* **2015**, *162*, A646.
- (17) Yao, X. Y.; Huang, N.; Han, F. D.; Zhang, Q.; Wan, H. L.; Mwizerwa, J. P.; Wang, C. S.; Xu, X. X.: High-Performance All-Solid-State Lithium-Sulfur Batteries Enabled by Amorphous Sulfur-Coated Reduced Graphene Oxide Cathodes. *Adv. Energy Mater.*, **2017**, *7*, 1602923.
- (18) Agostini, M.; Aihara, Y.; Yamada, T.; Scrosati, B.; Hassoun, J.: A Lithium–Sulfur Battery Using a Solid, Glass-Type P₂S₅–Li₂S electrolyte. *Solid State Ion.* **2013**, *244*, 48-51.

- (19) Lin, Z.; Liu, Z.; Fu, W.; Dudney, N. J.; Liang, C.: Lithium Polysulfidophosphates: A Family of Lithium-Conducting Sulfur-Rich Compounds for Lithium-Sulfur Batteries. *Angew. Chem. Int. Ed.*, **2013**, *52*, 7460-7463.
- (20) Lin, Z.; Liu, Z.; Dudney, N. J.; Liang, C.: Lithium Superionic Sulfide Cathode for All-Solid Lithium–Sulfur Batteries. *ACS Nano* **2013**, *7*, 2829-2833.
- (21) Zheng, M.; Tang, H.; Li, L.; Hu, Q.; Zhang, L.; Xue, H.; Pang, H.: Hierarchically Nanostructured Transition Metal Oxides for Lithium-Ion Batteries. *Adv. Sci.* **2018**, *5*, 1700592.
- (22) Li, B.; Gu, P.; Zhang, G.; Lu, Y.; Huang, K.; Xue, H.; Pang, H.: Ultrathin Nanosheet Assembled Sn_{0.91}Co_{0.19}S₂ Nanocages with Exposed (100) Facets for High-Performance Lithium-Ion Batteries. *Small* **2018**, *14*, 1702184.
- (23) Han, F.; Yue, J.; Fan, X.; Gao, T.; Luo, C.; Ma, Z.; Suo, L.; Wang, C.: High-Performance All-Solid-State Lithium-Sulfur Battery Enabled by a Mixed-Conductive Li₂S Nanocomposite. *Nano Lett.*, **2016**, *16*, 4521-4527.
- (24) Yue, J.; Han, F. D.; Fan, X. L.; Zhu, X. Y.; Ma, Z. H.; Yang, J.; Wang, C. S.: High-Performance All-Inorganic Solid-State Sodium-Sulfur Battery. *ACS Nano* **2017**, *11*, 4885-4891.
- (25) Richards, W. D.; Miara, L. J.; Wang, Y.; Kim, J. C.; Ceder, G.: Interface Stability in Solid-State Batteries. *Chem. Mat.*, **2016**, *28*, 266-273.
- (26) Suzuki, K.; Sakuma, M.; Hori, S.; Nakazawa, T.; Nagao, M.; Yonemura, M.; Hirayama, M.; Kanno, R.: Synthesis, Structure, and Electrochemical Properties of Crystalline Li-P-S-O Solid Electrolytes: Novel Lithium-Conducting Oxysulfides of Li₁₀GeP₂S₁₂ Family. *Solid State Ion.* **2016**, *288*, 229-234.

- (27) Nagao, M.; Suzuki, K.; Imade, Y.; Tateishi, M.; Watanabe, R.; Yokoi, T.; Hirayama, M.; Tatsumi, T.; Kanno, R.: All-Solid-State Lithium-Sulfur Batteries with Three-Dimensional Mesoporous Electrode Structures. *J. Power Sources* **2016**, *330*, 120-126.
- (28) Suzuki, K.; Kato, D.; Hara, K.; Yano, T. A.; Hirayama, M.; Hara, M.; Kanno, R.: Composite Sulfur Electrode Prepared by High-Temperature Mechanical Milling for Use in an All-Solid-State Lithium-Sulfur Battery with a Li_{3.25}Ge_{0.25}P_{0.75}S₄ Electrolyte. *Electrochimica Acta* **2017**, *258*, 110-115.
- (29) Trevey, J. E.; Gilsdorf, J. R.; Stoldt, C. R.; Lee, S. H.; Liu, P.: Electrochemical Investigation of All-Solid-State Lithium Batteries with a High Capacity Sulfur-Based Electrode. *J. Electrochem. Soc.* **2012**, *159*, A1019-A1022.
- (30) Tsukasaki, H.; Mori, Y.; Otoyama, M.; Yubuchi, S.; Asano, T.; Tanaka, Y.; Ohno, T.; Mori, S.; Hayashi, A.; Tatsumisago, M.: Crystallization Behavior of the Li₂S-P₂S₅ Glass Electrolyte in the LiNi_{1/3}Mn_{1/3}Co_{1/3}O₂ Positive Electrode Layer. *Sci. Rep.* **2018**, *8*, 6214.

TOC Figure

